Physics of Fluids

Active control of vortex-induced vibration of a circular cylinder using machine learning

Cite as: Phys. Fluids **31**, 093601 (2019); https://doi.org/10.1063/1.5115258
Submitted: 17 June 2019 • Accepted: 15 August 2019 • Published Online: 06 September 2019

Feng Ren, Chenglei Wang and Hui Tang

Physics of Fluids ARTICLE scitation.org/journal/phf

Active control of vortex-induced vibration of a circular cylinder using machine learning

Cite as: Phys. Fluids 31, 093601 (2019); doi: 10.1063/1.5115258
Submitted: 17 June 2019 • Accepted: 15 August 2019 •
Published Online: 6 September 2019

Feng Ren, Chenglei Wang, and Hui Tang[a)]

AFFILIATIONS

Research Center for Fluid-Structure Interactions, Department of Mechanical Engineering, The Hong Kong Polytechnic University, Kowloon, Hong Kong, China

[a)]Author to whom correspondence should be addressed: h.tang@polyu.edu.hk

ABSTRACT

We demonstrate the use of high-fidelity computational fluid dynamics simulations in machine-learning based active flow control. More specifically, for the first time, we adopt the genetic programming (GP) to select explicit control laws, in a data-driven and unsupervised manner, for the suppression of vortex-induced vibration (VIV) of a circular cylinder in a low-Reynolds-number flow (Re = 100), using blowing/suction at fixed locations. A cost function that balances both VIV suppression and energy consumption for the control is carefully chosen according to the knowledge obtained from pure blowing/suction open-loop controls. By implementing reasonable constraints to VIV amplitude and actuation strength during the GP evolution, the GP-selected best ten control laws all point to suction-type actuation. The best control law suggests that the suction strength should be nonzero when the cylinder is at its equilibrium position and should increase nonlinearly with the cylinder's transverse displacement. Applying this control law suppresses 94.2% of the VIV amplitude and achieves 21.4% better overall performance than the best open-loop controls. Furthermore, it is found that the GP-selected control law is robust, being effective in flows ranging from Re = 100 to 400. On the contrary, although the P-control can achieve similar performance as the GP-selected control at Re = 100, it deteriorates in higher Reynolds number flows. Although for demonstration purpose the chosen control problem is relatively simple, the training experience and insights obtained from this study can shed some light on future GP-based control of more complicated problems.

I. INTRODUCTION

Active flow control (AFC) has been hot in the field of fluid mechanics, in which a fluid system is purposely altered by actuators through exerting a small amount of energy input. Compared with passive control methods that usually involve geometrical changes, AFC is adaptive and hence can realize more effective control in a much wider operation range. Depending on whether the signals from the system output are fed back to regulate the actuator(s), AFC can be either open loop or closed loop.[1] Compared with open-loop control, closed-loop control can adjust actuation using feedback signals from the sensors and therefore can automatically operate in a much wider range. The control can be realized using either model-based methods or model-free methods. The former includes linear model,[2] stochastic model,[3] reduced order model,[4] etc., which have been successfully employed in many flow control problems. Take a classical control problem, i.e., vortex-induced vibration (VIV) suppression, as an example. Wang *et al.*[5] applied the proportional-integral control for windward-suction-leeward-blowing (WSLB)-based VIV suppression, suggesting that although the selected control strategies can completely suppress the VIV, the performance depends very much on the choices of control parameters.

Contrary to model-based methods, in model-free methods, the control law is derived in a data-driven and unsupervised manner. Among various methods in this type, a machine learning method, i.e., genetic programming (GP), has attracted great attention and has been successfully applied in AFC. Gautier *et al.*[6] first applied the GP to control the recirculation area of a backward-facing step. The optimal control law, converged after 12 generations, could reduce the recirculation area by 80%. Following this work, Debien *et al.*[7] used the GP control to mitigate separation and early reattachment of turbulent boundary layer from a sharp-edge ramp. In turbulent mixing layer manipulation experiments, Parezanovic *et al.*[8] showed that

the GP control can find the same intrinsic velocity signals essential for optimal control as those observed in reduced-order model-based feedback control. Furthermore, under the lock-on condition, they also demonstrated that the robustness of the GP control significantly outperforms open-loop controls when varying the freestream velocities.[9] Using another variant model of GP, i.e., the linear GP, Li *et al.*[10] conducted close-loop control tests for a car model and achieved a 22% drag reduction.

Note that the above GP-based AFCs were all realized in experiments, where the data-driven process can usually be conducted in a reasonable period of time. To our best knowledge, so far there is no GP-based AFC facilitated using high-fidelity computational fluid dynamics (CFD) simulations, probably due to very high computational costs associated with producing enough training data. However, with the rapid development of computing hardware and software, using CFD-simulated data for machine learning becomes readily feasible. Hence, in this study, we explore the use of high-fidelity CFD simulations to facilitate GP-based AFC. For demonstration purposes, we choose to control a VIV system vibrating in low Reynolds number flows. We understand that both open-loop and model-based controls have performed quite well in this type of problem. Hence, the purpose is not to showcase the superiority of machine learning-based control but to seek for the first time an alternative way to control this classical problem. The physical insights and training experience obtained from this study can shed some light on future GP-based control of more complicated problems.

II. PROBLEM DESCRIPTION AND METHODOLOGY

A. Problem description

VIV occurs when asymmetrical vortex pairs shed from a circular cylinder that is immersed in a uniform flow. Figure 1 shows a schematic of this fluid-structure interaction (FSI) problem. The velocity of the uniform incoming flow is U_0. The cylinder of diameter D_0 is connected to a spring in the transverse direction while being fixed in the streamwise direction.

The transverse motion of the cylinder is governed by

$$m\ddot{y} = -Ky + F_L, \tag{1}$$

where y is the transverse displacement, K is the stiffness of the spring, and F_L is the lift force. The dynamic response of the cylinder is mainly determined by two parameters, i.e., the mass ratio m^* and the reduced velocity U_R, defined as

$$m^* = \frac{m}{\rho_0 D_0^2}, \quad U_R = \frac{U_0}{f_N D_0}, \tag{2}$$

where $f_N = (K/m)^{1/2}/2\pi$ is the natural frequency of this mass-spring system in vacuum. In the present study, $m^* = 2$ and $U_R = 5$ are chosen, at which the system is operated in the lock-on region,[11] and hence, the VIV is difficult to suppress.[5,12–15]

To facilitate AFC, a pair of jets is applied on the cylinder's lee side. As depicted in Fig. 1, their angular position is set as $\gamma_{jet} = 70°$ and each jet slot consists of a 10° arc, which is slightly ahead of the mean separation point (i.e., 62.8°, with a variation of 2.9° according to Wu *et al.*[16]). It has been shown in our previous study that this setting is effective in influencing the development of vortices.[13]

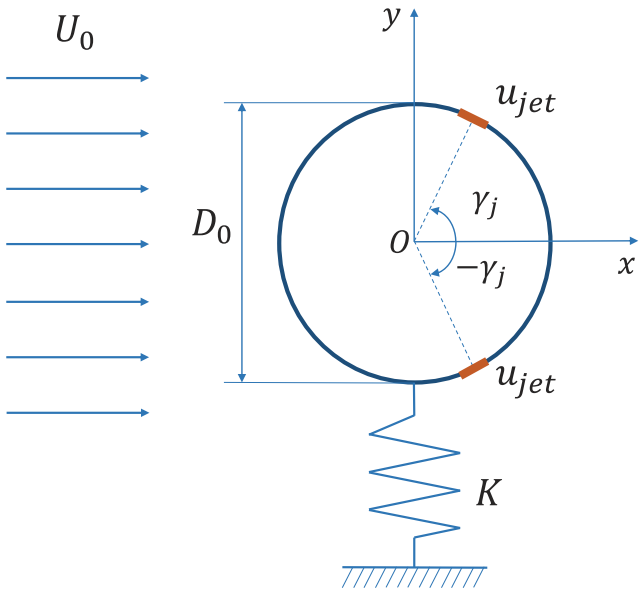

FIG. 1. Schematic of the VIV system. The jet pair is marked with two red arcs.

To reduce the parameter space, here we only focus on the control where the jet pair is issued with identical velocity along the streamwise direction. The velocity can be positive or negative, corresponding to the blowing or suction mode, respectively.

B. CFD solver and setup

In this study, unsteady CFD simulations are conducted to provide training data for GP-based machine learning. In the simulations, the fluid is treated incompressible and Newtonian. We adopt the lattice Boltzmann method (LBM) to numerically solve the Navier-Stokes equation, using an evolution procedure with separated collision and streaming steps. In this method, we use the multirelaxation time algorithm[17] to enhance numerical stability and the He-Luo model[18] to ensure fluid incompressibility.

Figure 2 shows a schematic of the computational domain, grid partition, and boundary conditions. The size of the computational domain is $64D_0 \times 20D_0$. The circular cylinder is initially located at the centerline, $20D_0$ downstream from the inlet. The multiblock grid partition method, proposed by Yu *et al.*,[19] is utilized to balance the computational accuracy and efficiency. We adopt a four-level grid refinement, where the mesh resolution is doubled from level 0 to level 3, each having uniform meshes.

We apply the Dirichlet boundary condition at the inlet and top/bottom walls, which is achieved via a modified bounce-back scheme with momentum exchange.[20] The inlet velocity is set as $U_0 = 0.02c$, where c is the lattice speed, corresponding to a time step $\delta t = T_0/3200$, where $T_0 = D_0/U_0$ is set as a reference time period. The convective flow condition, i.e., $\partial_t u + U_0 \partial_x u = 0$, is utilized at the outlet to allow the vortices to smoothly cross the boundary with the least reflection.[21] On the vibrating cylinder, we employ the double-linear interpolations for the treatment of curved boundary,[22] the third-order nonequilibrium extrapolation scheme for the

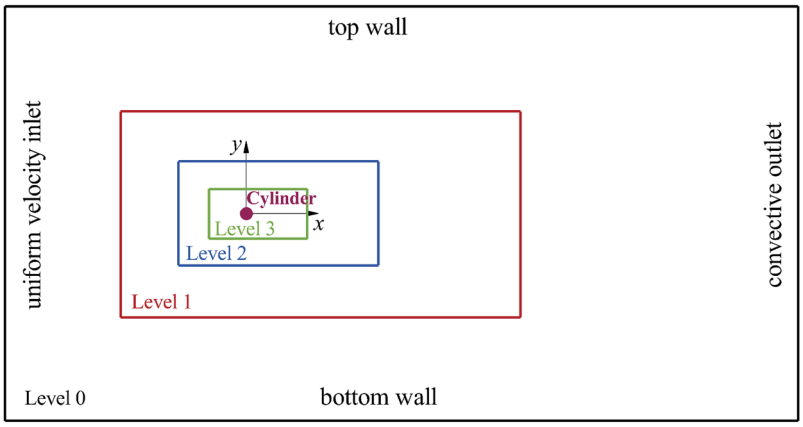

FIG. 2. Schematic of the computational domain, grid partition, and boundary conditions (not in scale).

mesh refilling process,[23] and the corrected momentum exchange method[24] to calculate the hydrodynamic forces.

Although via comparisons with various existing methods[25] the above simulation framework has been proven to be sufficiently accurate for simulating moving boundary problems, and the same grid partition and boundary setup have also been verified[13] and extensively used[5,14,15] in our previous studies, here we present additional mesh convergence and validation studies for simulated flow past a fixed or vibrating cylinder at Re = 100. Table I lists the results simulated using meshes of three different resolutions, together with. It is seen that in case II of the present study, where a mesh spacing of $\delta x = D_0/64$ is adopted in the Level 3 block, the mesh resolution is sufficient for both fixed and vibrating cylinder cases, with discrepancies of less than 1% in all concerned quantities (i.e., drag coefficient C_d, lift coefficient C_l, Strouhal number St, and cylinder vibration amplitude y_A) if compared with Case III, where the finest mesh is applied. These concerned quantities are also quite close to the results from the existing studies.[13,26,27] Hence, the set of mesh used in Case II is adopted in the current study.

C. GP control

The GP is a symbolic regression method in machine learning. Initially proposed by Koza,[28] this concept was inspired by the genetic algorithm (GA).[29] Although they share many common features, such as replication, crossover, mutation, the major difference between them is that the GP generates symbolic expressions using the locator/identifier separation protocol (LISP) language, while the GA only produces optimized values. The symbolic regression enables the GP to derive model-free controllers, where each symbolic expression becomes an explicit control law.

Figure 3 presents an outlook of the GP evolution framework for the AFC. Every GP-generated control law will be assessed by the FSI simulation module, which couples the fluid flow, single-freedom structure motion, and the jet-realized AFC. The outcome of the FSI simulation module, i.e., the cost function J [presented in Eq. (3)], will then be sent back to the GP selection module. After the assessment is done for all control laws in one generation, they will be ranked according to their J values. The best few control laws generating smallest J values are chosen to produce the candidate control laws of the next generation using the GP.

The parameters used in the current GP evolution are listed in Table II, which are similar to those in Li *et al.*[10] To generate symbolic expressions, the GP includes four basic algebraic operators (i.e., +, −, ×, ÷) and four transcendental functions (i.e., sin, cos, log, tanh). Here, the transcendental functions are chosen to introduce nonlinear characteristics. Specifically, sine and cosine functions introduce periodicity, the hyperbolic tangent function sets a threshold value, and logarithm brings in slowly or rapidly varying trends at certain

TABLE I. Mesh convergence and validation studies for simulated flow past a fixed or vibrating cylinder at Re = 100.

Case		Mesh resolution (Level 3)	$D_0/\delta x$	Fixed cylinder C_d	Fixed cylinder C_l	Fixed cylinder St	Vibrating cylinder with $m^* = 2$ and $U_R = 5$ y_A	Vibrating cylinder with $m^* = 2$ and $U_R = 5$ St
Present study	I	256 × 128	32	1.350 ± 0.009	±0.325	0.167	±0.474	0.182
	II	512 × 160	64	1.374 ± 0.011	±0.338	0.169	±0.522	0.186
	III	1024 × 320	128	1.375 ± 0.011	±0.341	0.169	±0.527	0.186
Russell and Wang[26]		...	...	1.38 ± 0.007	±0.332	0.169	...	...
Choi *et al.*[27]		...	...	1.34 ± 0.011	±0.315	0.164	...	...
Wang *et al.*[13]		...	60	...	±0.337	0.169	±0.545	0.186

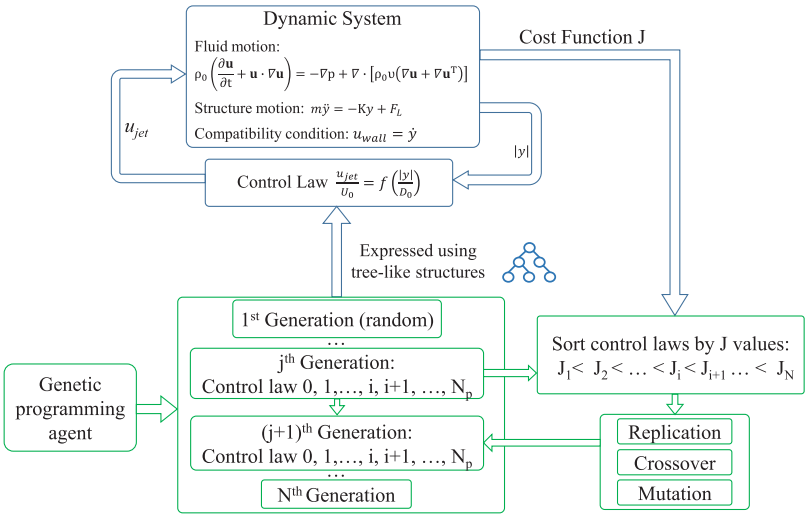

FIG. 3. Schematic of the GP evolution framework for the AFC.

ranges of the argument. Note that we did not include the exponential or power function in order to avoid sharp changes in the control outputs.

It is generally assumed that, given sufficiently large population size and after a sufficient number of generations, the GP evolution can converge to globally optimal individuals. Though not having been rigorously proved due to the complexity in symbolic operations, this assumption has been well proved for the GA.[30] In this study, we choose to let the learning process evolve for 25 generations, each containing a population of 50 members. Initially, the population members are given random expressions, and the depth of tree-like symbolic structures ranges from 2 to 6. Once the evaluation of all 50 members, i.e., candidate control laws, in one generation is completed, they will be sorted according to their cost function values. The best 5 members generating smallest J values, i.e., 5 tournaments, are then chosen to produce all 50 members in the next generation. During this evolution, three principal genetic operations are employed, i.e., replication, crossover, and mutation. First, the 5 tournaments can replicate themselves to participate in competitions in the next generation. Second, they also get a chance to breed, so that their children can inherit the genes from two excellent parents and could possibly perform better than their parents. This is a process called crossover [as depicted in Fig. 4(a)]. Last, the tournaments may also experience mutations, in which a part of the tree-like expression structure happens to be replaced by another randomly produced expression. Three typical mutation modes, i.e., subtree mutation, hoist mutation, and point mutation, are adopted in this study, as depicted in Figs. 4(b)–4(d).

In the current GP evolution framework, the probabilities for replication, crossover, and mutation are set as 0.1, 0.3, and 0.6, respectively. Here, we adopt a large mutation probability to ensure the diversity in a generation of a limited population size. In addition, to avoid producing very lengthy symbolic expressions, the parsimony coefficient is set as 0.001. More detailed information about the GP can be found in Poli *et al.*[31] and Pedregosa *et al.*[32]

During the GP evolution process for learning optimum control laws, the most time-consuming procedure is the FSI simulation due to the high-fidelity CFD simulations and numerous cases involved (in total, 1250 cases for a 25-generation evolution). To save the time, we applied the graphics processing unit (GPU) acceleration technique, which is capable of improving the efficiency by an order of 10^2, as has been shown in our previous study.[33] The FSI simulations were performed on a main node with a Xeon E5-2620 CPU together with a Tesla K40c GPU. The evaluation of each case only took about 22 min, which can be further reduced if more powerful hardware is used.

TABLE II. Parameters used in the GP selection module.

GP setup	Parameter values
Number of generations	25
Population size	50
Tournament size	5
Operators	+, −, ×, ÷, sin, cos, log, tanh
Constant range	[−1, 1]
Mutation probability	0.6
Replication probability	0.1
Crossover probability	0.3
Parsimony coefficient	0.001

III. RESULTS AND DISCUSSIONS

A. Open-loop control

To provide prerequisite information for the machine learning-based closed-loop control, we first conduct open-loop controls, where two types of actuation are applied, i.e., pure blowing and pure suction, with constant velocities. The temporal histories of the cylinder's transverse displacement are compared in Fig. 5(a), where $t/T_0 = 0$ corresponds to the instant when the cylinder is fixed and its surrounding flow achieves the dynamic steady state and $t/T_0 = 10$ corresponds to the instant when the cylinder is released to vibrate and the actuators start to operate. It is seen that the pure blowing can consistently mitigate the VIV, and the control improves with

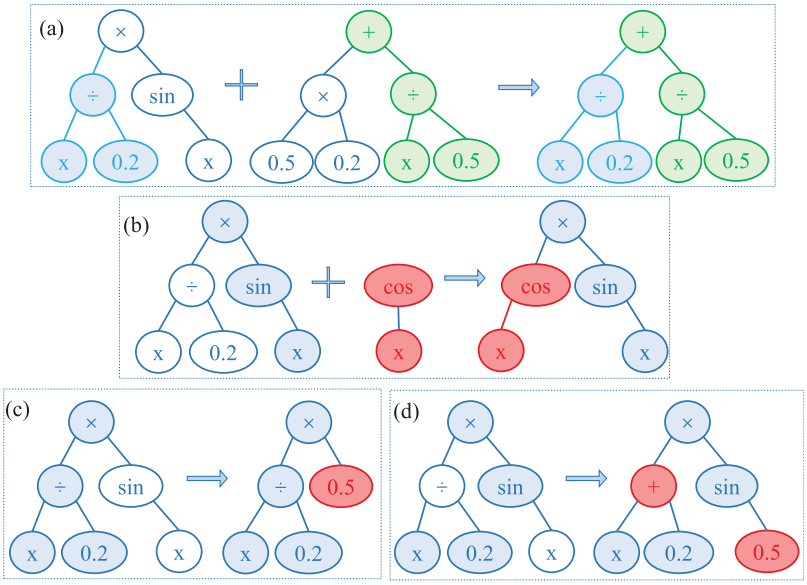

FIG. 4. Examples of main modes in generating new populations: (a) crossover, (b) subtree mutation, (c) hoist mutation, (d) point mutation.

the blowing strength. But for the pure suction control, the VIV can only be mitigated when the actuation is strong enough, i.e., $|u_{jet}| \geq 3U_0$. When weak suction (i.e., $|u_{jet}| \leq 2U_0$) is applied, the VIV is even worse off compared with the uncontrolled case.

The observed difference in the control effects between the pure blowing and pure suction is believed to be related to the interaction of these fluidic manipulations with the development of shear layers and resulting vortices. In the pure blowing control, the issuing jets tend to interrupt the development of shear layers, causing early shedding of vortices. As such, compared with the uncontrolled case, the vortices shed at a higher frequency as revealed in Figs. 5(b) and 5(c). Furthermore, it is seen from Fig. 5(c) that the issuing jets tend to slice the vortices into small pieces, which then merge again with weaker strength. These weakened vortices then induce smaller lift and smaller VIV amplitude.

In the pure suction control, the fluidic entrainment tends to stabilize the shear layers, allowing them to develop for a longer time and evolve into stronger vortices. As such, the vortices shed at a lower frequency as revealed in Figs. 5(b) and 5(d). If the suction is relatively weak, such as in the $u_{jet} = -U_0$ and $-2U_0$ cases, the stronger vortices are close enough to the cylinder, inducing larger lift and larger VIV amplitude. However, if the suction is strong enough, such as in the $|u_{jet}| \geq 3U_0$ case, the stabilized shear layers are maintained for a much longer distance, forming vortices that are already far away from the cylinder, as confirmed in Fig. 5(d). Hence, the resulting lift and VIV amplitude become significantly smaller.

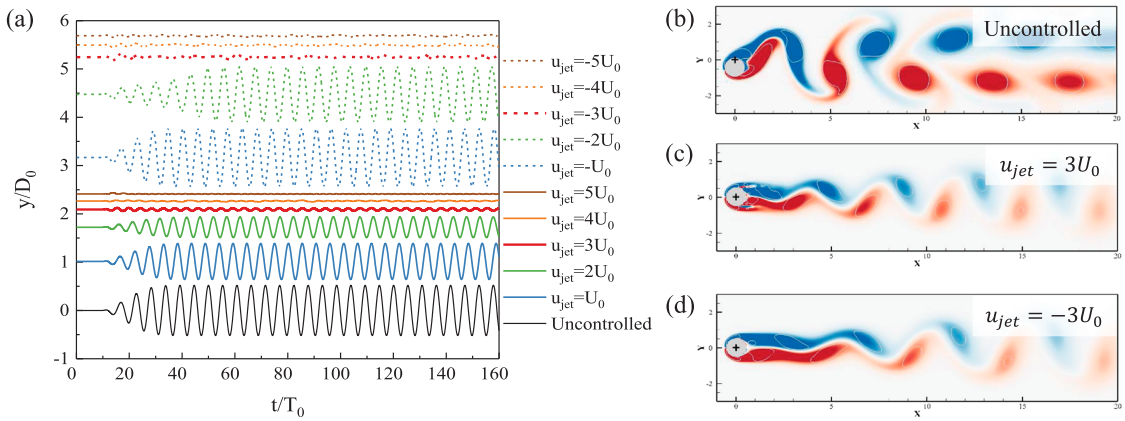

FIG. 5. (a) Temporal variations in the cylinder's transverse displacement, where for clarity, each data set is shifted up from its lower neighbor. Instantaneous vorticity distribution in (b) the uncontrolled case, (c) the blowing case with $u_{jet} = 3U_0$, and (d) the suction case with $u_{jet} = -3U_0$. The vorticity is normalized by T_0 and is scaled to the [−0.2, 0.2] interval. The gray lines denote vortices using the λ_{ci} criterion,[34] with $\lambda_{ci} = 0.1$. The symbol "+" denotes the equilibrium position of the cylinder.

From these results, it can be concluded that the minimum required actuation strength that makes both types of actuation effective is about $|u_{jet}| = 3U_0$, with which the pure blowing and the pure suction can reduce the VIV amplitude by 94.8% and 94.4%, respectively, if compared with that in the uncontrolled case.

If the actuation strength is further increased, the improvement in the VIV mitigation becomes marginal. Thus, the energy expenditure due to the actuation should be taken into account to evaluate the overall control performance. Below, we introduce a cost function considering both effectiveness and efficiency of the control:

$$J = J_1 + J_2 = \frac{1}{\Delta t}\int_{t_0}^{t_0+\Delta t}\frac{|y|^2}{D_0^2}dt + \frac{C}{\Delta t}\int_{t_0}^{t_0+\Delta t}\frac{u_{jet}^2}{U_0^2}dt. \quad (3)$$

The cost function J consists of two parts: J_1 reflects the mean square of VIV amplitude over a selected long period Δt and J_2 reflects the mean energy consumed by the blowing/suction actuation during the same period. In this study, the evaluation of the cost function starts from $t_0 = 80T_0$ and lasts for a period $\Delta t = 50T_0$. This selected period allows the cylinder to freely oscillate for about 9 uncontrolled cycles, which is enough for the evaluation of the averaged control performance.

In Eq. (3), J_2 is weighed with a coefficient C, which is determined by the results of the current open-loop controls. Since the control with $u_{jet} = \pm 3U_0$ can drastically reduce the VIV amplitude and further increasing the actuation strength only slightly improves the control while consuming much more energy, we deem that $u_{jet} = \pm 3U_0$ is the best choice and hence set C = 0.002 to ensure the minimization of the corresponding J values. As shown in Fig. 6, the J values in the $u_{jet} = \pm 3U_0$ case, i.e., 0.018 36 and 0.018 43, are the smallest among all cases. Therefore, the cost function defined in Eq. (3) and the weighting coefficient C = 0.002 are adopted in the subsequent close-loop controls.

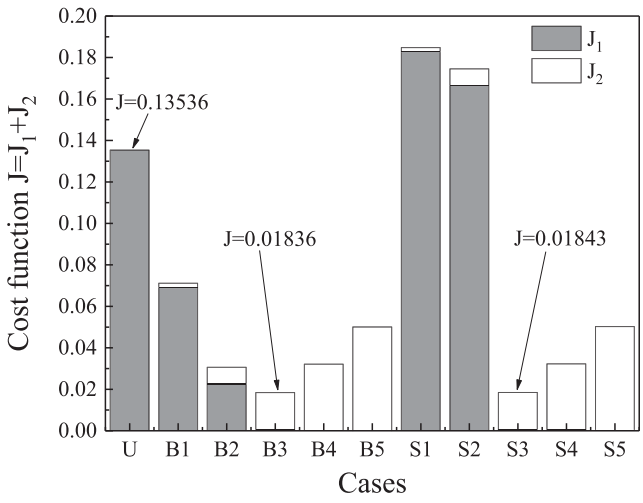

FIG. 6. Comparison of the open-loop controls by considering both VIV suppression and energy consumption, where in the x-axis, "U" denotes the uncontrolled case, "B" denotes blowing cases, and "S" denotes suction cases, and the number reflects the actuation strength.

B. GP control

To ensure the generation of reasonable controls, two constraints are enforced during the GP selection process. That is, when evaluating each candidate control law, the FSI simulation will be terminated if the VIV amplitude exceeds $0.6D_0$ (i.e., slightly larger than that in the uncontrolled case) or if the actuation velocity exceeds $4.5U_0$ (i.e., 50% higher than $u_{jet} = \pm 3U_0$ in the best open-loop controls). A very large J value will then be assigned to this control law to ensure that it no longer contributes to the proceeding generation.

The evolution process is shown in Fig. 7, where each dot represents a candidate control law. For the sake of better presentation, a small number of control laws that produce J > 0.2 are not shown. About 79% of control laws appear under the blue dashed line that represents the uncontrolled case, and about 27% of control laws appear under the green dashed-dotted line that represents the best open-loop control case (with $u_{jet} = 3U_0$). The evolution process proceeds for 25 generations. As depicted by the red line in Fig. 7, the minimum cost function value in each generation quickly converges after just three generations. The control law with the overall minimum cost function value, i.e., J = 0.014 69, appears in the 13th generation.

Figure 8(a) presents ten best control laws. It is intriguing to see that all these ten control laws use suction-type actuation. Except for one that corresponds to uniform suction, these control laws exhibit a similar trend, i.e., the suction strength is nonzero when the cylinder is at its equilibrium position (i.e., y = 0) and increases nonlinearly with the cylinder's transverse displacement. Among them, the best control law is

$$\frac{u_{jet}}{U_0} = 1 - 3.637\cos^{-1}\left(\frac{|y|}{D_0}\right). \quad (4)$$

With this control law being implemented, the jet actuation and the cylinder's dynamic response are examined in Fig. 8(b). Compared

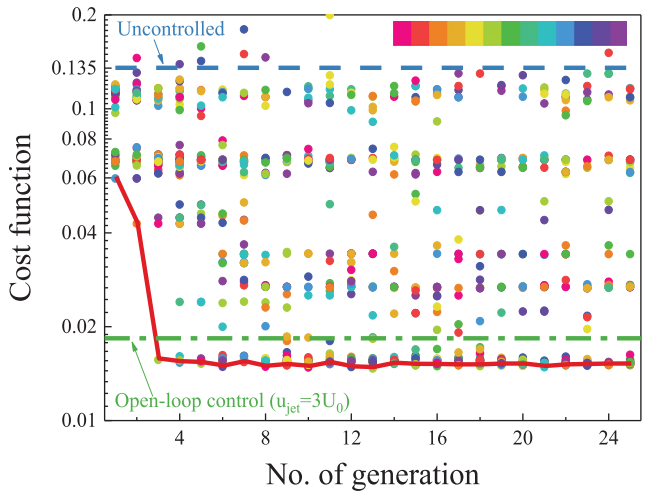

FIG. 7. GP evolution process, where the red solid line describes the trend of minimum cost function values, the blue dashed line represents the uncontrolled case, and the green dashed-dotted line represents the best open-loop control. Colors of the circular symbols are arranged according to their appearance sequence in each generation.

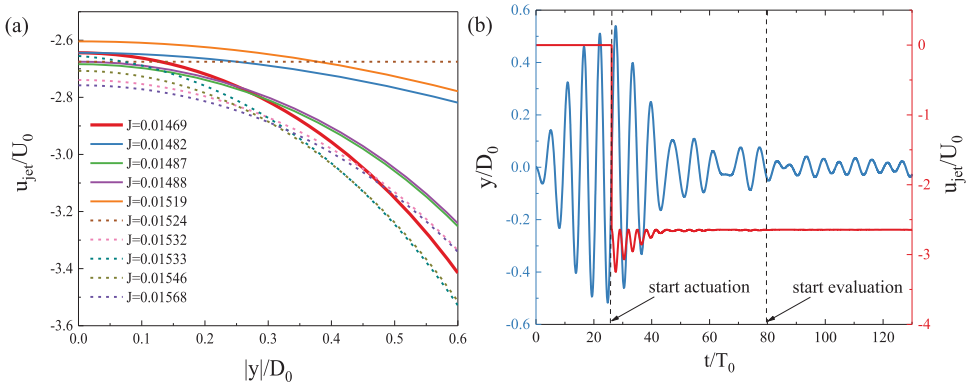

FIG. 8. (a) Ten best control laws selected by the GP method. (b) Evolution of the actuation strength and the cylinder's transverse location in the case controlled by the best control law.

with the uncontrolled case, the VIV amplitude is reduced by 94.2%, a value close to that in the best open-loop control cases ($u_{jet} = \pm 3U_0$). However, compared with the best open-loop control cases, the optimal GP controller further reduces the energy cost by 22.2% and hence achieves a much better overall performance with the J value reduced by 21.4%.

A question may arise from the above finding that the GP-selected best control laws all point to suction-type actuation: is it inevitable or just caused by an initial bias introduced at the beginning of the GP evolution? To address this issue, we conducted another set of GP evolution, in which the settings remain the same but only the blow-type actuation is enforced. As shown in Fig. 9(a), the evolution lasts for 10 generations, and the minimum cost function value quickly converges after just 4 generations. The best control law with the overall minimum cost function value J = 0.016 25 appears in the 7th generation, which is 11.5% smaller than the best open-loop blowing control (i.e., with $u_{jet} = 3U_0$) but 10.6% larger than the best control selected in the first set of GP evolution [i.e., the control described by Eq. (4)]. The corresponding control law is shown in Fig. 9(b), suggesting that the blowing velocity first increases rapidly with the cylinder's transverse displacement to a peak of about $3.3U_0$ at $|y| \approx 0.05D_0$ and then gradually decreases, quite different from the best suction-type controls shown in Fig. 8(a). Controlled with this law, the cylinder's VIV amplitude is similar to that controlled by Eq. (4), as shown in Fig. 10(a). However, Fig. 10(b) reveals that the blowing velocity oscillates violently between $1.4U_0$ and $3.2U_0$, a consequence of the rapid change near the cylinder's equilibrium position (i.e., y = 0) as suggested in Fig. 9(b). This violent velocity oscillation is responsible for a higher energy expenditure and hence a higher overall cost function value. From this supplementary study, we confirm that under the current settings, the overall best control laws being the suction-type actuation is inevitable.

C. Comparison with P control

To further evaluate the GP-based VIV control, we compare the GP-selected optimal controller [i.e., Eq. (4)] with conventional linear control techniques, i.e., the proportional integral differential (PID) control. Since our previous study has revealed that the P or I control alone is eligible to completely suppress the VIV,[5] here we only choose the P control for the comparison, which can be described as

$$\frac{u_{jet}}{U_0} = P\frac{|y|}{D_0}. \tag{5}$$

Like the GP control, the P control also gives an explicit relationship between the actuation velocity and cylinder's transverse displacement. However, it enforces a rigid linear relationship. A number of P values ranging from −80 to 100 are tested. To avoid unrealistic actuation strength, we also limit the actuation velocity magnitude within $4.5U_0$.

Figure 11 shows the variation in cost function values against the P values. It is seen that for the P values studied herein, J_1 monotonically decreases with the absolute P value, indicating that

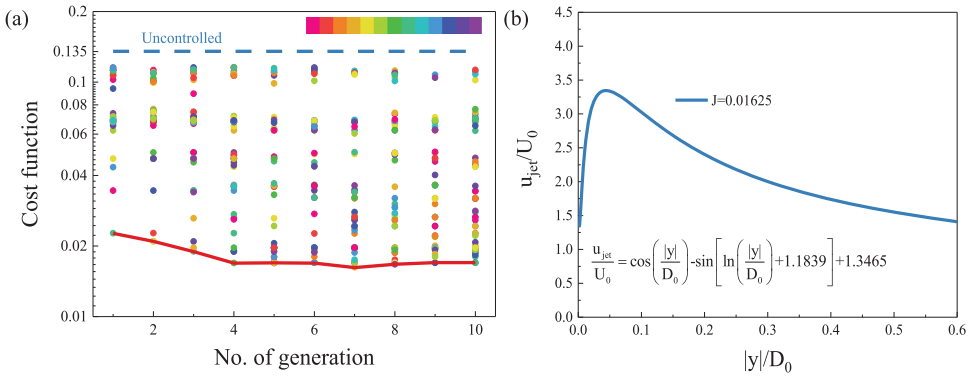

FIG. 9. (a) GP evolution process with only blow-type controls enforced, where the red solid line describes the trend of minimum cost function values and the blue dashed line represents the uncontrolled case. Colors of the circular symbols are arranged according to their appearance sequence in each generation. (b) The best blow-type control law selected by the GP method.

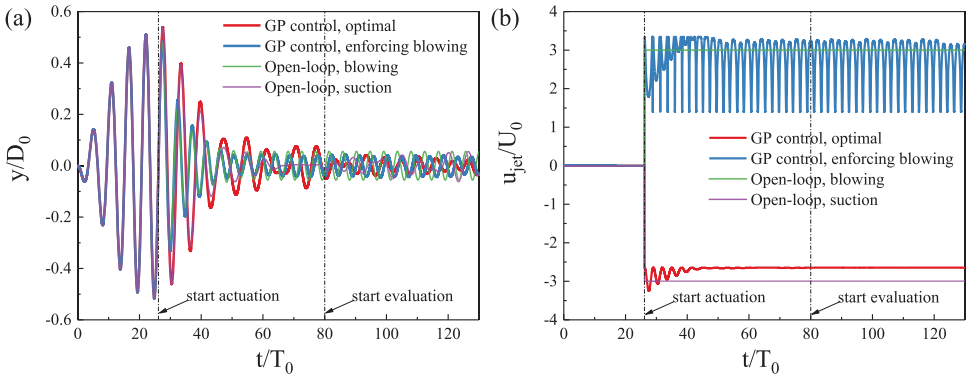

FIG. 10. Evolution of (a) the cylinder's transverse position and (b) the actuation velocity for the cases with the GP-selected best control law, the best blow-type control law, and the two best open-loop control laws.

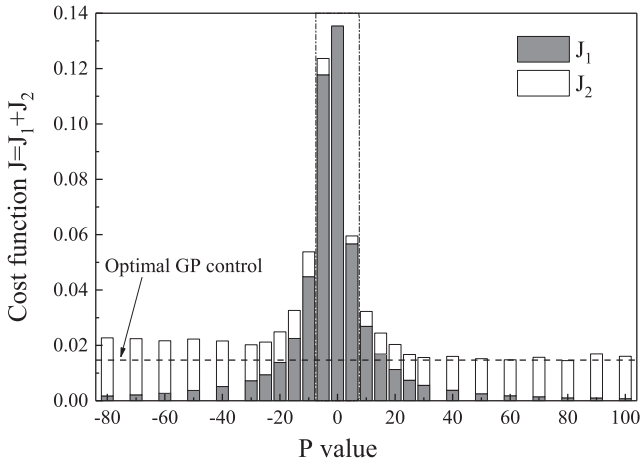

FIG. 11. Variation in the P control cost function values against the P values, where the dashed line represents the value of the best GP-selected control. In the histogram, the region between the two vertical dashed-dotted lines denotes cases that the control does not reach the velocity constraint. The uncontrolled case, i.e., the P = 0 case, is also shown for comparison purpose.

the cylinder's VIV amplitude reduces with |P|. It is also interesting to see that at the same |P| value, the blow-type control (with positive P) suppresses more VIV than the suction-type control (with negative P). Different from J_1, if taking the energy consumption into account, the overall cost function J slightly fluctuates when |P| > 30, due to the enforcement of the actuation strength constraint. From these results, it can be concluded that the P control can suppress the VIV well. In the best case, i.e., the case with P = 80, the control can suppress the VIV amplitude by 91.2%, and the total cost function J approaches the value in the best GP-selected control.

D. Robustness at larger Reynolds numbers

Robustness is an important issue for control laws. Similar to what has been reported in Gautier *et al.*,[6] in this section, we will assess the robustness of the best GP-selected control law [i.e., Eq. (4)] and the best P control law [i.e., Eq. (5) with P = 80] as well as the best open-loop controls (i.e., with $u_{jet} = \pm 3U_0$) by evaluating their performance at various Reynolds numbers. CFD simulations at higher Reynolds numbers were conducted by linearly increasing the spatial and temporal resolutions. For instance, at Re = 400, 2048 × 640 grid nodes were used for each of the four grid blocks, and 6400 time steps were used in each T_0 period.

The cost function values obtained from different control strategies at the Reynolds numbers ranging from 100 to 400 are plotted in Fig. 12. Figure 12(a) shows that the GP control and the open-loop controls can all remarkably suppress the VIV at Re > 100, despite that the control becomes slightly less effective at Re = 100. Compared with these controls, the P control performs relatively poorly, especially at higher Reynolds numbers. If the energy consumption is taken into account, it is seen from Fig. 12(b) that in general the GP

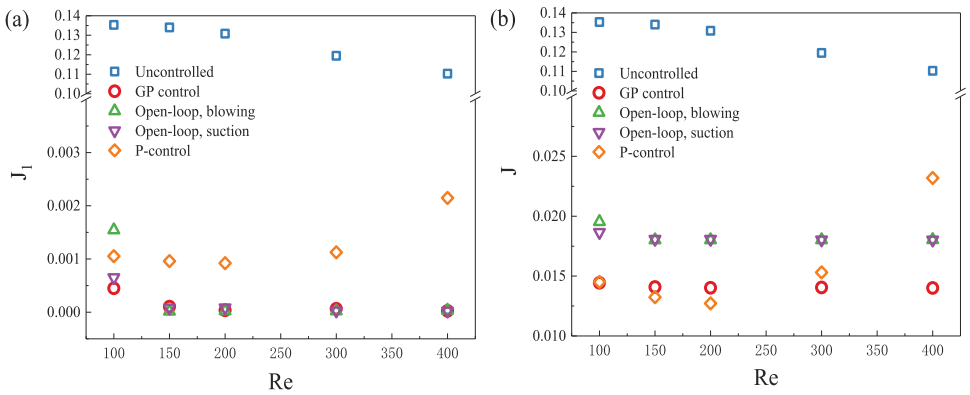

FIG. 12. Variation in (a) J_1 and (b) J of different controls against the Reynolds number ranging from 100 to 400, where the open-loop controls is conducted with $u_{jet} = \pm 3U_0$ and the P control uses P = 80.

control performs the best and is very robust, maintaining low J values at all Reynolds numbers. The open-loop controls are also robust, not affected too much by the Reynolds number. On the contrary, the P control is much affected. It obtains the overall smallest J value at Re = 200 while obtaining the overall largest J value at Re = 400. These results indicate that the GP control is not only effective and efficient but also robust, suitable for VIV control under various flow conditions.

IV. SUMMARY

In this study, we demonstrate the use of high-fidelity CFD simulations in machine learning-based AFC. For the first time, we adopt the GP method to select the best explicit control laws, in a data-driven and unsupervised manner, for the suppression of a VIV system vibrating in a low Reynolds number flow (Re = 100). Being weighted according to the prior knowledge obtained from pure blowing/suction open-loop controls, the chosen cost function takes both VIV amplitude and energy expenditure for the control into consideration. Another set of closed-loop control using a linear controller, i.e., the P control, is also conducted for comparison purposes. The major conclusions are summarized as follows:

(1) With the implementation of the GPU acceleration technique, it is now feasible to run a large number of high-fidelity CFD simulations to facilitate machine learning-based AFC.
(2) The current GP evolution process converges very fast, after just three generations. It is interesting to see that by implementing the constraints for maximum allowed VIV magnitude ($0.6D_0$) and maximum allowed actuation strength ($4.5U_0$), the GP-selected best ten control laws all use suction-type actuation. The best control law [i.e., Eq. (4)] suggests that the suction strength should be nonzero when the cylinder is at its equilibrium position and should increase nonlinearly with the cylinder's transverse displacement. It is effective and efficient in the VIV control, suppressing the VIV amplitude by 94.2%, meanwhile reducing the energy cost by 22.2% if compared with the best open-loop controls.
(3) The GP control is robust in flows ranging from Re = 100 to 400. Although the P control at Re = 100 can achieve similar performance as the GP-selected control, it deteriorates at Reynolds numbers higher than 300.

Note that due to the randomness involved in generating initial population and mutation during the evolution, in different runs the GP evolution may produce best control laws in different expressions. But the level of minimum cost function after the convergence is achieved should not be affected too much. Although the selected VIV problem to be controlled is relatively simple, the training experience and insights obtained from this study can shed some light on future GP-based control of more complicated problems.

In real conditions, it may be difficult to find enough reliable data for machine learning, which can be caused by either high costs or very rough measurements in practical experiments. Since literally CFD simulations do not have physical constraints, with the fast advancement of computing power and artificial intelligence (AI) algorithms, hopefully in the near future much more complex engineering problems can be solved with relative ease using this framework.

ACKNOWLEDGMENTS

We gratefully acknowledge the financial support for this study from Research Grants Council of Hong Kong under General Research Fund (Project Nos. 15249316 and 15214418) and the Departmental General Research Fund (Project No. G-YBXQ). We would also like to acknowledge the University Research Facility in Big Data Analytics (UBDA) of The Hong Kong Polytechnic University for providing high-performance computing resources. In addition, the work is based on our inhouse CFD code, with the open-source application programming interface (API) *gplearn* on the GitHub (*https://github.com/trevorstephens/gplearn*) shared by Trevor Stephens.

REFERENCES

[1] S. S. Collis, R. D. Joslin, A. Seifert, and V. Theofilis, "Issues in active flow control: Theory, control, simulation, and experiment," Prog. Aerosp. Sci. **40**, 237–289 (2004).
[2] J. Kim and T. R. Bewley, "A linear systems approach to flow control," Annu. Rev. Fluid Mech. **39**, 383–417 (2007).
[3] R. D. Brackston, J. M. G. de la Cruz, A. Wynn, G. Rigas, and J. F. Morrison, "Stochastic modelling and feedback control of bistability in a turbulent bluff body wake," J. Fluid Mech. **802**, 726–749 (2016).
[4] C. W. Rowley and S. T. M. Dawson, "Model reduction for flow analysis and control," Annu. Rev. Fluid Mech. **49**, 387–417 (2017).
[5] C. L. Wang, H. Tang, S. C. M. Yu, and F. Duan, "Active control of vortex-induced vibrations of a circular cylinder using windward-suction-leeward-blowing actuation," Phys. Fluids **28**, 053601 (2016).
[6] N. Gautier, J. L. Aider, T. Duriez, B. R. Noack, M. Segond, and M. Abel, "Closed-loop separation control using machine learning," J. Fluid Mech. **770**, 442–457 (2015).
[7] A. Debien, K. von Krbek, N. Mazellier, T. Duriez, L. Cordier, B. R. Noack, M. W. Abel, and A. Kourta, "Closed-loop separation control over a sharp edge ramp using genetic programming," Exp. Fluids **57**, 40 (2016).
[8] V. Parezanovic, J.-C. Laurentie, C. Fourment, J. Delville, J.-P. Bonnet, A. Spohn, T. Duriez, L. Cordier, B. R. Noack, M. Abel, M. Segond, T. Shaqarin, and S. L. Brunton, "Mixing layer manipulation experiment from open-loop forcing to closed-loop machine learning control," Flow, Turbul. Combust. **94**, 155–173 (2015).
[9] V. Parezanovic, L. Cordier, A. Spohn, T. Duriez, B. R. Noack, J. P. Bonnet, M. Segond, M. Abel, and S. L. Brunton, "Frequency selection by feedback control in a turbulent shear flow," J. Fluid Mech. **797**, 247–283 (2016).
[10] R. Y. Li, B. R. Noack, L. Cordier, J. Boree, and F. Harambat, "Drag reduction of a car model by linear genetic programming control," Exp. Fluids **58**, 103 (2017).
[11] W. W. Zhang, X. T. Li, Z. Y. Ye, and Y. W. Jiang, "Mechanism of frequency lock-in in vortex-induced vibrations at low Reynolds numbers," J. Fluid Mech. **783**, 72–102 (2015).
[12] L. Du and X. F. Sun, "Suppression of vortex-induced vibration using the rotary oscillation of a cylinder," Phys. Fluids **27**, 023603 (2015).
[13] C. L. Wang, H. Tang, F. Duan, and S. C. M. Yu, "Control of wakes and vortex-induced vibrations of a single circular cylinder using synthetic jets," J. Fluids Struct. **60**, 160–179 (2016).
[14] C. L. Wang, H. Tang, S. C. M. Yu, and F. Duan, "Lock-on of vortex shedding to a pair of synthetic jets with phase difference," Phys. Rev. Fluids **2**, 104701 (2017).
[15] C. L. Wang, H. Tang, S. C. M. Yu, and F. Duan, "Control of vortex-induced vibration using a pair of synthetic jets: Influence of active lock-on," Phys. Fluids **29**, 083602 (2017).
[16] M. H. Wu, C. Y. Wen, R. H. Yen, M. C. Weng, and A. B. Wang, "Experimental and numerical study of the separation angle for flow around a circular cylinder at low Reynolds number," J. Fluid Mech. **515**, 233–260 (2004).

[17]D. d'Humieres, I. Ginzburg, M. Krafczyk, P. Lallemand, and L. S. Luo, "Multiple-relaxation-time lattice Boltzmann models in three dimensions," Philos. Trans. R. Soc. London, Ser. A **360**, 437–451 (2002).
[18]X. Y. He and L. S. Luo, "Lattice Boltzmann model for the incompressible Navier-Stokes equation," J. Stat. Phys. **88**, 927 (1997).
[19]D. Yu, R. Mei, and S. Wei, "A multi-block lattice Boltzmann method for viscous fluid flows," Int. J. Numer. Methods Fluids **39**, 99–120 (2002).
[20]A. J. C. Ladd, "Numerical simulations of particulate suspensions via a discretized Boltzmann equation. 1. Theoretical foundation," J. Fluid Mech. **271**, 285–309 (1994).
[21]A. Fakhari and T. Lee, "Finite-difference lattice Boltzmann method with a block-structured adaptive-mesh-refinement technique," Phys. Rev. E **89**, 033310 (2014).
[22]D. Z. Yu, R. W. Mei, L. S. Luo, and W. Shyy, "Viscous flow computations with the method of lattice Boltzmann equation," Prog. Aerosp. Sci. **39**, 329–367 (2003).
[23]A. Caiazzo, "Analysis of lattice Boltzmann nodes initialisation in moving boundary problems," Prog. Comput. Fluid Dyn. **8**, 3–10 (2008).
[24]Y. Chen, Q. D. Cai, Z. H. Xia, M. R. Wang, and S. Y. Chen, "Momentum-exchange method in lattice Boltzmann simulations of particle-fluid interactions," Phys. Rev. E **88**, 013303 (2013).
[25]S. Tao, J. J. Hu, and Z. L. Guo, "An investigation on momentum exchange methods and refilling algorithms for lattice Boltzmann simulation of particulate flows," Comput. Fluids **133**, 1–14 (2016).
[26]D. Russell and Z. J. Wang, "A cartesian grid method for modeling multiple moving objects in 2D incompressible viscous flow," J. Comput. Phys. **191**, 177–205 (2003).
[27]J. I. Choi, R. C. Oberoi, J. R. Edwards, and J. A. Rosati, "An immersed boundary method for complex incompressible flows," J. Comput. Phys. **224**, 757–784 (2007).
[28]J. R. Koza, *Genetic Programming: On the Programming of Computers by Means of Natural Selection* (MIT Press, Cambridge, MA, 1992).
[29]D. E. Goldberg and J. H. Holland, "Genetic algorithms and machine learning," Mach. Learn. **3**, 95–99 (1988).
[30]R. F. Hartl and R. Belew, *A Global Convergence Proof for a Class of Genetic Algorithms* (University of Technology, Vienna, 1990).
[31]R. Poli, W. B. Langdon, N. F. McPhee, and J. R. Koza, *A Field Guide to Genetic Programming* (Lulu Enterprises, UK Ltd., 2008).
[32]F. Pedregosa, G. Varoquaux, A. Gramfort, V. Michel, B. Thirion, O. Grisel, M. Blondel, P. Prettenhofer, R. Weiss, and V. Dubourg, "Scikit-learn: Machine learning in python," J. Mach. Learn. Res. **12**, 2825–2830 (2011), available at http://www.jmlr.org/papers/v12/pedregosa11a.html.
[33]F. Ren, B. W. Song, Y. Zhang, and H. B. Hu, "A GPU-accelerated solver for turbulent flow and scalar transport based on the lattice Boltzmann method," Comput. Fluids **173**, 29–36 (2018).
[34]J. Zhou, R. J. Adrian, S. Balachandar, and T. M. Kendall, "Mechanisms for generating coherent packets of hairpin vortices in channel flow," J. Fluid Mech. **387**, 353–396 (1999).